pISSN 2384-1095
eISSN 2384-1109

iMRI 2017;21:71-81

https://doi.org/10.13104/imri.2017.21.2.71

iMRI
Investigative Magnetic Resonance Imaging

Comparison of Three, Motion-Resistant MR Sequences on Hepatobiliary Phase for Gadoxetic Acid (Gd-EOB-DTPA)-Enhanced MR Imaging of the Liver

Doo Ri Kim[1], Bong Soo Kim[1], Jeong Sub Lee[1], Guk Myung Choi[1], Seung Hyoung Kim[1], Myeng Ju Goh[1], Byung-Cheol Song[2], Mu Sook Lee[1], Kyung Ryeol Lee[1], Su Yeon Ko[1]

[1]Department of Diagnostic Radiology, Jeju National University Hospital, Jeju, Korea
[2]Department of Internal Medicine, Jeju National University Hospital, Jeju, Korea

Original Article

Received: March 12, 2017
Revised: April 2, 2017
Accepted: April 18, 2017

Correspondence to:
Bong Soo Kim, M.D.
Department of Radiology,
Jeju National University Hospital,
Jeju National University School of Medicine, 15, Aran 13-gil, Jeju-si, Jeju Special Self-governing Province 63241, Korea.
Tel. +82-64-717-1373
Fax. +82-64-717-1372
E-mail: 671228kbs@naver.com

Purpose: To compare three, motion-resistant, T1-weighted MR sequences on the hepatobiliary phase for gadoxetic acid-enhanced MR imaging of the liver.

Materials and Methods: In this retrospective study, 79 patients underwent gadoxetic acid-enhanced, 3T liver MR imaging. Fifty-nine were examined using a standard protocol, and 20 were examined using a motion-resistant protocol. During the hepatocyte-specific phase, three MR sequences were acquired: 1) gradient recalled echo (GRE) with controlled aliasing in parallel imaging results in higher acceleration (CAIPIRINHA); 2) radial GRE with the interleaved angle-bisection scheme (ILAB); and 3) radial GRE with golden-angle scheme (GA). Two readers independently assessed images with motion artifacts, streaking artifacts, liver-edge sharpness, hepatic vessel clarity, lesion conspicuity, and overall image quality, using a 5-point scale. The images were assessed by measurement of liver signal-to-noise ratio (SNR), and tumor-to-liver contrast-to-noise ratio (CNR). The results were compared, using repeated post-hoc, paired t-tests with Bonferroni correction and the Wilcoxon signed rank test with Bonferroni correction.

Results: In the qualitative analysis of cooperative patients, the results for CAIPIRINHA had significantly higher ratings for streak artifacts, liver-edge sharpness, hepatic vessel clarity, and overall image quality as compared to, radial GRE, ($P < 0.016$). In the imaging of uncooperative patients, higher scores were recorded for ILAB and GA with respect to all of the qualitative assessments, except for streak artifact, compared with CAIPIRINHA ($P < 0.016$). However, no significant differences were found between ILAB and GA. For quantitative analysis in uncooperative patients, the mean liver SNR and lesion-to-liver CNR with radial GRE were significantly higher than those of CAIPIRINHA ($P < 0.016$).

Conclusion: In uncooperative patients, the use of the radial GRE sequence can improve the image quality compared to GRE imaging with CAIPIRINHA, despite the data acquisition methods used. The GRE imaging with CAIPIRINHA is applicable for patients without breath-holding difficulties.

Keywords: Liver; Magnetic resonance imaging; Breath-holding; Gadolinium ethoxybenzyl DTPA

INTRODUCTION

Recent technical development has dramatically improved the quality of liver magnetic resonance (MR) imaging for the detection and characterization of lesions (1-6). Until fairly recently, T1-weighted, 3-dimensional (3D), volumetric, interpolated breath-holding examination techniques, using Cartesian k-space sampling are most widely used as contrast-enhanced liver MR examinations in routine clinical practice. The image quality of this technique depends on the appropriateness of the patient's breath holding (3-6). In uncooperative patients, this sequence is sensitive to motion artifacts, which can make it difficult to detect lesions.

Various methods have been proposed to achieve optimal images for image creation before deterioration of image quality by reducing acquisition time. The newly developed, parallel acceleration technique (3D gradient recalled echo [GRE], with controlled aliasing in parallel imaging, resulting in higher acceleration [CAIPIRINHA]), can save image acquisition time, by modifying the phase encoding sampling manner, which leads to reduced aliasing artifacts and provides better image quality, although patients cannot hold their breath long enough (7-10). Therefore, this rapid imaging technique that reduces respiration artifacts, may propel patients with short breathing capacity, into routine clinical MR practice.

Currently, another method for minimizing patient motion, are the radial k-space sampling schemes, such as the 3D radial GRE. Using this technique, k-space lines are collected in a radial fashion, resulting in high sampling of the central k-space and motion artifact suppression (1, 11-15). There are two radial GRE sequences, the interleaved, angle-bisection scheme (ILAB), and the golden-angle scheme (GA) (13). ILAB obtains radial spokes with short angular distances in consecutive order, while GA obtains radial spokes with large angular distances in serial order (13). Until now there has been no clinical study which demonstrated better performance for acquiring high quality, than the 3D GRE with CAIPIRINHA technique compared with the 3D radial GRE sequence (ILAB and GA acquisitions) for gadoxetic, acid-enhanced MR imaging of the liver. Therefore, the purpose of our study is to compare the 3D GRE with the CAIPIRINHA technique and the 3D, radial GRE sequences on the hepatobiliary phase of liver MR imaging and to determine the most appropriate sequence for uncooperative patients.

MATERIALS AND METHODS

Study Population

Our Institutional Review Board (IRB) approved this HIPAA-compliant, retrospective study and waived informed consent (IRB number: 2017-02-001). The MR imaging database was retrospectively searched for the records of patients who underwent liver MR examinations that included gadoxetic acid-enhancement, the 3D T1-weighted GRE, using the CAIPIRINHA technique, and the 3D T1-weighted GRE with radial sampling sequences at 3T. The study group consisted of 79, consecutive, registered patients (48 males, 31 females; mean age 67 ± [13.4] years; age range, 17-87 years). The primary indication for imaging included the evaluation of patients with cirrhosis (n = 36) and non-cirrhotic, chronic viral hepatitis (n = 10), who underwent imaging for the surveillance or evaluation of hepatocellular carcinoma (n = 46), hepatic metastasis work-up (n = 28), evaluation of cholangiocarcinoma (n = 4), and differential diagnosis of a hepatic cystic mass (n = 1). Among the liver cirrhosis group which was clinically diagnosed, liver function was classified using the Child-Pugh score (Grade A, 33; Grade B, 1; Grade C, 2).

MR Examination

Liver MR imaging was performed using a 3T MR scanner (Skyra; Siemens Medical Systems, Erlangen, Germany) and a 32-channel, phased-array coil with one of two protocols, i.e. standard or motion-resistant protocol. Among the 79 patients, 59 were examined using the standard protocol, and 20 were examined using the motion-resistant protocol. The two, patient groups were classified by the scanning technologist after precontrast, and T1-weighted imaging using the in-phase/out-of-phase sequence was acquired. If patients could follow instructions and hold their breath during image acquisition, they were classified as cooperative patients and examined by standard protocol. However, if patients had difficulty with breath-holding (mental status, age, underlying lung disease, hearing ability, and pain), that resulted in severe motion artifacts on the breath-holding T1-weighted, dual echo sequence, they were classified as uncooperative patients and examined by motion-resistant protocol.

Table 1 shows our standard liver MR imaging protocol for cooperative patients and motion-resistant protocol for uncooperative patients. Our standard liver MR imaging protocol consisted of a breath-holding, T1-weighted, dual-echo (in-phase and opposed phase) sequence, dynamic

fat-saturated, 3D T1-weighted GRE sequence, using the CAIPIRINHA technique and the 3D T1-weighted radial GRE sequence using k-space weighted image contrast (KWIC) technique, a breath-holding, fat-saturated T2-weighted turbo spin-echo sequence, or the single-shot, echo-train, spin-echo (SS-ETSE) technique. Dynamic imaging, including the arterial phase, the portal venous phase, and the delayed phase, was performed before and after injection of gadoxetic disodium (Gd-EOB-DTPA) (Primovist; Bayer Healthcare, Berlin, Germany). The standard dose of contrast (0.025 mmol/kg) was intravenously administered as a 0.1 mL/kg (body weight) at a rate of 1.2 mL/s, and was immediately followed by a 20-mL saline flush through an antecubital venous catheter using a power injector (Spectris Solaris EP; Medrad, Warrendale, PA, USA). The multiple arterial phases (four arterial phases) were acquired using the 3D T1-weighted radial GRE sequence using KWIC during 20 seconds after the arrival of contrast medium at the aortic arch under real-time monitoring. Each arterial phase acquisition was 5 seconds in duration. The portal venous phase and the delayed phase were acquired at 70 seconds and 3 minutes. Our motion-resistant, liver MR imaging protocol for uncooperative patients, consisted of a magnetization-prepared, rapid-acquisition gradient echo (MP-RAGE) with dual echo, dynamic fat-saturated, 3D T1-weighted radial GRE sequence using KWIC technique, SS-ETSE. The multiple arterial phases (four arterial phases) in uncooperative patients were acquired using a 3D T1-weighted radial GRE sequence using KWIC in the same methods used in cooperative patients. After that, a free breathing, T1-weighted radial GRE sequence started at 70 seconds after initiation of contrast material injection. This phase acquisition in the middle of the portal venous and delayed phases was approximately 3 minutes in duration. Twenty minutes after the intravenous injection of gadoxetic acid, a breath-holding, 3D GRE VIBE with CAIPIRINHA image, free breathing 3D radial GRE sequence with GA acquisition, and free breathing 3D radial GRE sequence with ILAB acquisition were subsequently acquired using both protocols. Patients were instructed to breath in a normal manner during 3D radial GRE acquisitions. One thousand and twenty-four radial spokes were acquired. The MRI sequence parameters on hepatobiliary phase are summarized in Table 2.

Image Analysis

Qualitative Analysis

Two radiologists (B.S.K. and S.H.K) with 17 years and 13 years, respectively, of clinical experience interpreting

Table 1. Standard and Motion-Resistant Protocols at a 3.0T MR Scanner

	Standard protocol	Motion-resistant protocol
Dual echo (in-phase and opposed phase)	Breath hold, T1-weighted dual-echo sequence	Free breathing, T1-weighted MP-RAGE with dual-echo sequence
Dynamic imaging		
Precontrast phase	Breath hold, fat-saturated T1-weighted 3D GRE VIBE with CAIPIRINHA	Free breathing, fat-saturated T1-weighted 3D radial GRE with GA
Arterial phase	Breath hold, fat-saturated T1-weighted radial 3D-GRE with KWIC technique	Breath hold, fat-saturated T1-weighted radial 3D-GRE with KWIC technique
Portal venous phase	Breath hold, fat-saturated T1-weighted 3D GRE VIBE with CAIPIRINHA	Free breathing, fat-saturated T1-weighted 3D radial GRE with GA
3 minute delayed phase	Breath hold, fat-saturated T1-weighted 3D GRE VIBE with CAIPIRINHA	
Hepatobiliary imaging	Breath hold, fat-saturated T1-weighted 3D GRE VIBE with CAIPIRINHA	Breath hold, Fat-saturated T1-weighted 3D GRE VIBE with CAIPIRINHA
	Free breathing fat-saturated T1-weighted 3D radial GRE with GA	Free breathing fat-saturated T1-weighted 3D radial GRE with GA
	Free breathing fat-saturated T1-weighted 3D radial GRE with ILAB	Free breathing fat-saturated T1-weighted 3D radial GRE with ILAB
T2-weighted imaging	Breath hold, fat-saturated TSE sequence or SS-ETSE	SS-ETSE

CAIPIRINHA = controlled aliasing in parallel imaging results in a higher acceleration; GA = golden angle; GRE = gradient-recalled echo; ILAB = interleaved angle-bisection; KWIC = k-space weighted image contrast technique; MP-RAGE = magnetization prepared, rapid-acquisition gradient echo; SS-ETSE = single-shot, echo-train, spin-echo; TSE = turbo spin echo; VIBE = volumetric interpolated breath-hold examination

Table 2. Parameters of Motion-Resistant Sequences Used at a 3.0T MR Scanner

Parameters	3D GRE VIBE with CAIPIRINHA	Radial 3D-GRE with GA	Radial 3D-GRE with ILAB
TR (milliseconds)	5	3	3
TE (milliseconds)	2	2	2
Flip angle (^{0})	12	12	12
Slice thickness (mm)	2.5	2.5	2.5
Matrix size	384 × 241	384 × 384	384 × 384
FOV	303 × 305 mm	340 × 340	340 × 340
Acquisition time (sec)	14 sec	167 sec	167 sec
Fat suppression	Fat saturated	Fat saturated	Fat saturated
Respiratory control	BH	BI	BI

BH = breath-hold; BI = breathing-independent; CAIPIRINHA = controlled aliasing in parallel imaging results in a higher acceleration; FOV = field of view; GA = golden angle; GRE = gradient-recalled echo; ILAB = interleaved angle-bisection; TE = echo time; TR = repetition time; VIBE = volumetric interpolated breath-hold examination

abdominal MR's, independently evaluated the three image sets. All images were reviewed using the picture archiving and communication system (Infinitt PACS; Infinitt Healthcare, Seoul, Korea). Both radiologists were blinded to the image acquisition technique, clinical information, and image reading records.

For each data set, each reader determined the motion artifact, streaking artifact, liver edge sharpness, hepatic vessel clarity, lesion conspicuity, and overall image quality using a 5-point scale. Motion artifact and streaking artifacts were graded as 5, no visible artifact as 4, minimal artifact as 3, moderate visible artifact as 2, and severe visible artifact as 1, visible artifact which renders the image of no diagnostic value. Liver edge sharpness was graded as 5, excellent; 4, good; 3, fair; 2, poor; and 1, unacceptable. Intrahepatic vessel clarity was scored according to the degree of the depiction of the peripheral hepatic vessel: 5, sharp and clearly demarcated; 4, mild blurring; 3, moderate blurring; 2, substantial blurring; and 1, uninterpretable because of severe blurring. The readers evaluated the conspicuity of focal liver lesions. When a patient had multiple focal lesions, the evaluation was assessed for the previously determined largest one detected on whole MR sequences. If the largest lesion was less than 1 cm in diameter, it was excluded. Forty-six focal liver lesions were evaluated in our study. Thirty-one patients had malignant lesions (hepatocellular carcinoma [n = 23], metastasis [n = 4], intrahepatic mass-forming cholangiocarcinoma [n = 3] or combined hepatocellular carcinoma and cholangiocarcinoma [n = 1]). Fifteen patients had benign lesions (hemangioma [n = 10], cyst [n = 2], abscess [n = 2] or focal nodular hyperplasia [n = 1]). The final diagnosis of focal liver lesions was based on the histologic findings, clinical evidence, typical CT and MRI findings, and laboratory findings. For each identified lesion, the lesion conspicuity was assessed considering the lesion visibility, margin, and detectability: 5, very good, diagnostic; 4, good; 3, fair, diagnostic; 2, poor, non-diagnostic; and 1, uninterpretable, non-diagnostic. The overall image quality was assessed using all of the above considerations: 5, Very good, diagnostic; 4, good; 3, fair, diagnostic; 2, poor, non-diagnostic; and 1, uninterpretable, non-diagnostic.

Quantitative Analysis

A radiologist (D.R.K.) evaluated the region-of-interest (ROI) of the image sets for quantitative image analysis. This radiologist did not participate in the qualitative image analysis. The shape and size of the ROIs were identical for all of the three images. The ROI was placed within homogenous portions of each organ and away from vessels and necrosis. The signal intensity (SI) of ROIs from the normal liver parenchyma, lesion (for the previously determined largest one), and mesenteric fat, and the standard deviation (SD) of the background and mesenteric fat were measured. The signal-to-noise ratio (SNR) of liver (SI_{liver}/SD_{noise}) and lesion-to-liver, contrast-to-noise ratio (CNR) ($[SI_{lesion} - SI_{liver}]/SD_{noise}$) were calculated.

Statistical Analysis

The Friedman nonparametric test was used to assess statistically significant differences of qualitative data obtained from the comparative analysis of 3D GRE with CAIPIRINHA, 3D radial GRE with GA, and 3D radial ILAB. For those parameters in which a statistically significant

difference in ratings was observed, a comparison between pairs of sequences was made using the Wilcoxon signed rank test with Bonferroni correction. Interobserver reproducibility for the qualitative data was assessed using kappa statistics. A weighted kappa value less than 0.2 indicated slight agreement, 0.21–0.40 fair agreement, 0.41–0.60 moderate agreement, 0.61–0.80 good agreement, and greater than 0.81 excellent agreement. To analyze the quantitative data of the three sequences, a repeated measures analysis of variance test was performed. The differences between the pairs of the sequences were compared using the post-hoc paired t-test with Bonferroni correction. A value of $P < 0.05$ indicated a statistically significant difference. A value of $P < 0.016$ was regarded as statistically significant as Bonferroni correction for multiple comparisons was applied. The statistical analyses

Table 3. Results of Qualitative Analysis of Three, Motion-Resistant Sequences in Cooperative Patients

Parameters	3D GRE VIBE with CAIPIRINHA	3D radial GRE		P^a			P^b
		GA	ILAB	3D GRE VIBE with CAIPIRINHA vs. 3D radial GRE with GA	3D GRE VIBE with CAIPIRINHA vs. 3D radial GRE with ILAB	3D radial GRE with GA vs. 3D radial GRE ILAB	
Motion artifact	4.82 ± 0.36	4.76 ± 0.28	4.77 ± 0.27	NA	NA	NA	0.057
Streak artifact	5.00 ± 0.00	4.39 ± 0.53	4.31 ± 0.56	< 0.001*	< 0.001*	0.15	< 0.001*
Sharpness of liver edge	4.83 ± 0.32	4.46 ± 0.52	4.49 ± 0.51	< 0.001*	< 0.001*	0.305	< 0.001*
Clarity of intrahepatic vessel	4.42 ± 0.87	4.19 ± 0.81	4.26 ± 0.80	0.002*	0.013*	0.101	0.001*
Lesion conspicuity	4.54 ± 0.83	4.34 ± 0.68	4.32 ± 0.68	0.071	0.039	0.608	< 0.001*
Overall image quality	4.75 ± 0.49	4.41 ± 0.61	4.39 ± 0.64	< 0.001*	< 0.001*	0.647	< 0.001*

Values are the mean ± standard deviation. NA: Wilcoxon signed rank test was not available.

Wilcoxon signed rank test with Bonferroni correction was used for comparison between pairs of sequences. P^a Results were considered statistically significant at $P^a < 0.016$.

Friedman nonparametric test was used for statistical analysis of the three sequences. P^b Results were considered statistically significant at $P^b < 0.05$.

* Statistically significant

CAIPIRINHA = controlled aliasing in parallel imaging results in a higher acceleration; GA = golden angle; GRE = gradient-recalled echo; ILAB = interleaved angle-bisection; VIBE = volumetric interpolated breath-hold examination

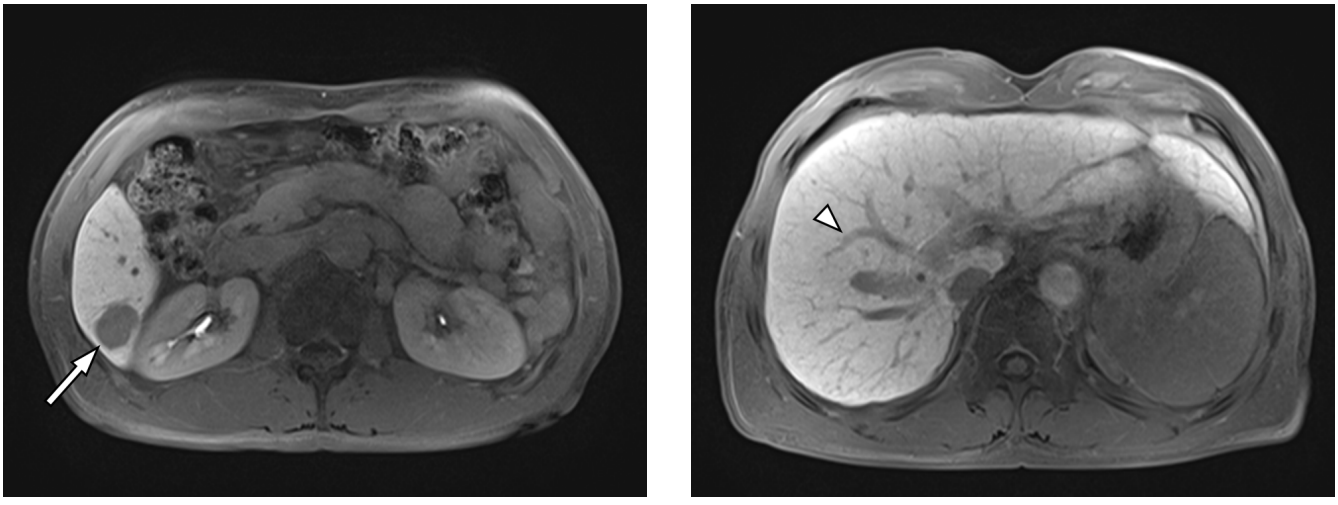

a b

Fig. 1. MR images of a 59-year-old man with hepatocellular carcinoma. He had one hepatocellular carcinoma in liver segment 6. A hepatocellular carcinoma (arrow) in the liver is clearly shown on the axial breath-hold, T1-weighted 3D GRE image with CAIPIRINHA (a) in this cooperative patient. The intrahepatic vessel (arrowhead) is well-visualized in the T1-weighted 3D GRE image with CAIPIRINHA (b).

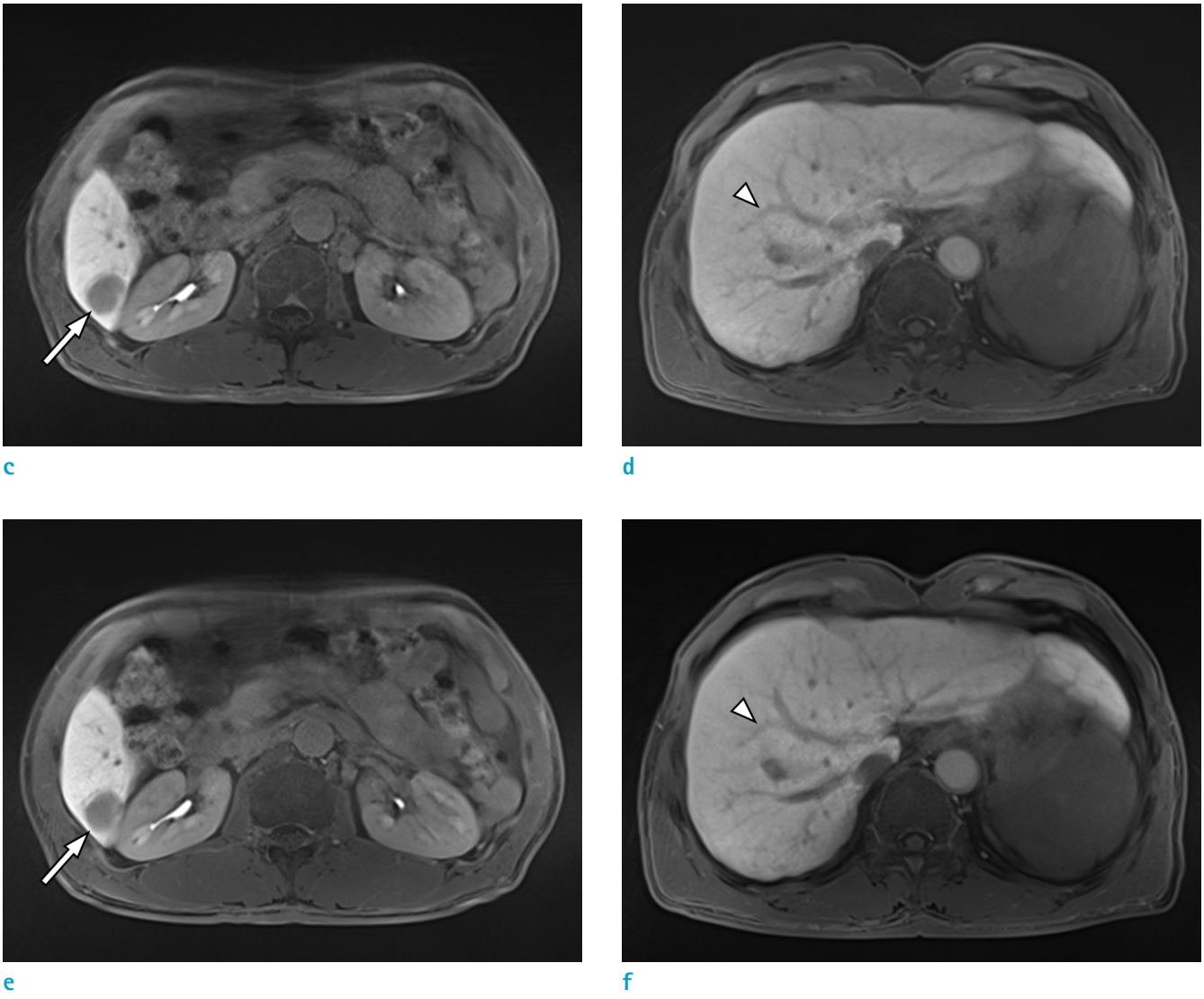

Fig. 1. Axial free-breathing 3D radial GRE with GA (c, d) and 3D radial GRE with ILAB (e, f) show blurred resolution of the tumor (arrows) and margin of the intrahepatic vessel (arrowheads).

were conducted using SPSS software (version 18.0; SPSS, Chicago, IL, USA).

RESULTS

Qualitative Analysis

For qualitative analysis in cooperative patients, the 3D GRE with CAIPIRINHA was mostly superior to the 3D radial GRE with GA and the 3D radial GRE with ILAB. The streak artifact, sharpness of the liver edge, clarity of intrahepatic vessels, and overall image quality of 3D GRE with CAIPIRINHA was significantly higher than those of either the 3D radial GRE with GA or 3D radial GRE ILAB ($P < 0.016$). Images obtained with the 3D GRE with CAIPIRINHA were of slightly better motion artifact scores and lesion conspicuity than those obtained with either 3D radial GRE with GA, or 3D radial GRE ILAB, although not with statistical significance ($P > 0.016$) (Table 3, Fig. 1). However, both 3D radial GRE with GA and 3D radial GRE ILAB had adequate image quality with a mean score always rated higher than 4 (good to very good or minimal artifacts) in all qualitative parameters. There were no significant differences between 3D radial GRE with GA, and 3D radial GRE with ILAB for all of the qualitative parameters ($P > 0.016$).

On the contrary, in uncooperative patients, the 3D, radial

GRE with GA and 3D radial GRE with ILAB had better quality than the 3D GRE with CAIPIRINHA in all items except the streak artifact, and there was a statistically significant difference between any of the two, 3D radial GRE sequences and the 3D GRE with CAIPIRINHA ($P < 0.016$) (Table 4, Fig. 2). The clarity of intrahepatic vessels and lesion conspicuity on 3D GRE with CAIPIRINHA were rated lower than 3 (a mean rating of 2.75 and 2.73, respectively). There was no significant difference between 3D radial GRE with GA and 3D radial GRE with ILAB for all qualitative parameters ($P > 0.016$). The weighted kappa values for the two reviewers, which were calculated on the basis of each interpreter's qualitative data, were 0.67 in cooperative patients and 0.70 in uncooperative patients (moderate to good agreement), respectively.

Quantitative Analysis

The quantitative analysis results in cooperative patients are shown in Table 5. The mean liver SNR with 3D radial GRE with ILAB were higher than those with 3D radial GRE with GA and 3D GRE with CAIPIRINHA. The mean lesion-to-liver CNR was highest with 3D radial GRE with ILAB, followed by 3D radial GRE with GA and 3D GRE with CAIPIRINHA, although there is no statistical significance between any two sequences ($P > 0.05$). Both the 3D radial GRE with GA and the 3D radial GRE with ILAB provided more homogenous fat suppression than 3D GRE with CAIPIRINHA. The fat percentage SD of SI with the 3D radial GRE sequence with GA and 3D radial with ILAB was significantly lower than that with 3D GRE with CAIPIRINHA ($P < 0.001$).

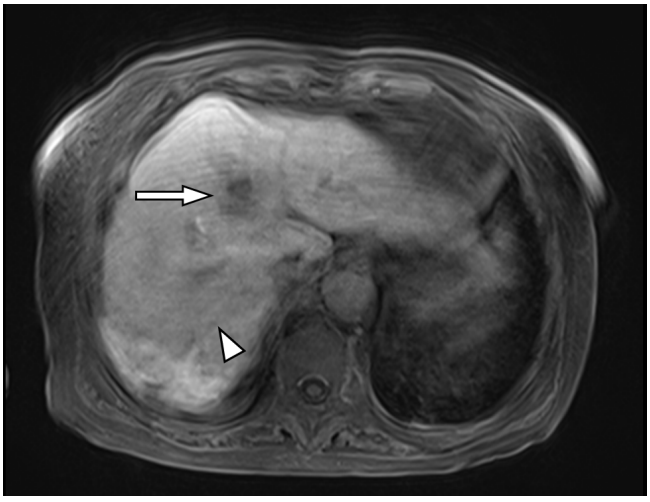

a

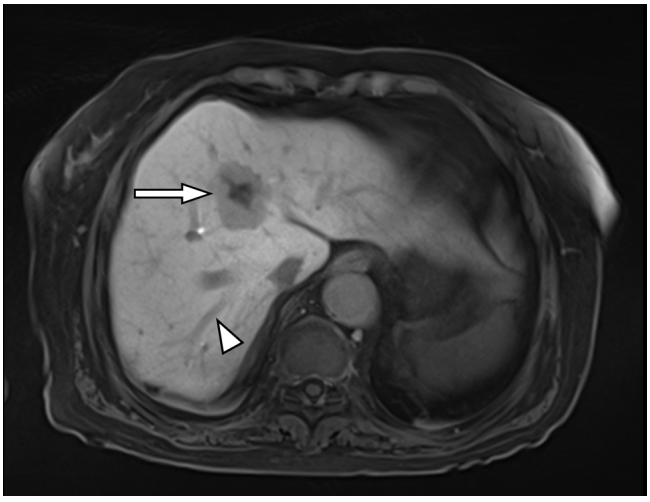

b

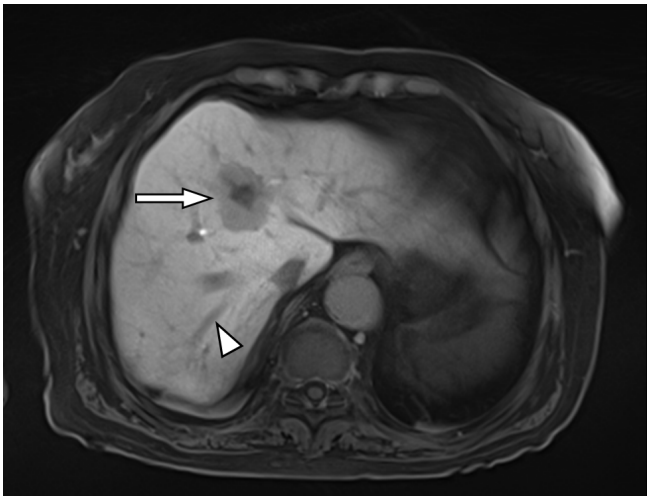

c

Fig. 2. MR images in a 75-year-old woman with intrahepatic, mass-forming cholangiocarcinoma. She had one intrahepatic, mass-forming cholangiocarcinoma in liver segments 4 and 8. Axial breath-hold, T1-weighted 3D GRE image with CAIPIRINHA (a) shows severe motion artifacts due to the patient's breathing. Axial free-breathing, 3D radial GRE with GA (b) and 3D radial GRE with ILAB (c) demonstrate substantially artifact reduction resistance to motion and high image quality in the patient who could not suspend respiration. The intrahepatic, mass-forming cholangiocarcinoma (arrows) and intrahepatic vessels (arrowheads) are better depicted in axial free-breathing, 3D radial GRE with GA and 3D radial GRE with ILAB.

The quantitative analysis results in uncooperative patients are shown in Table 6. The mean liver SNR and lesion-to-liver CNR with 3D radial GRE with ILAB and 3D radial GRE with GA were significantly higher than those of 3D GRE with CAIPIRINHA. For malignant lesions, the 3D radial GRE sequences had better lesion-to-liver CNR than the 3D GRE with CAIPIRINHA (P = 0.003 and 0.004, respectively). Regarding the quantitative assessment of fat, the 3D radial

Table 4. Results of Qualitative Analysis of Three, Motion-Resistant Sequences in Uncooperative Patients

Parameters	3D GRE VIBE with CAIPIRINHA	3D radial GRE		P^a			P^b
		GA	ILAB	3D GRE VIBE with CAIPIRINHA vs. 3D radial GRE with GA	3D GRE VIBE with CAIPIRINHA vs. 3D radial GRE with ILAB	3D radial GRE with GA vs. 3D radial GRE ILAB	
Motion artifact	3.18 ± 0.71	4.58 ± 0.34	4.55 ± 0.32	< 0.001*	< 0.001*	0.317	< 0.001*
Streak artifact	5.00 ± 0.00	4.23 ± 0.53	4.25 ± 0.50	< 0.001*	< 0.001*	0.813	< 0.001*
Sharpness of liver edge	3.20 ± 0.70	4.13 ± 0.51	4.15 ± 0.49	0.002*	0.001*	0.785	< 0.001*
Clarity of intrahepatic vessel	2.75 ± 0.66	3.83 ± 0.75	3.80 ± 0.80	< 0.001*	< 0.001*	0.564	< 0.001*
Lesion conspicuity	2.73 ± 0.67	4.12 ± 0.58	4.12 ± 0.62	0.002*	0.001*	1	< 0.001*
Overall image quality	3.03 ± 0.68	4.13 ± 0.58	4.15 ± 0.61	0.001*	0.001*	0.792	< 0.001*

Values are the mean ± standard deviation. NA: Wilcoxon signed rank test was not available.
Wilcoxon signed rank test with Bonferroni correction was used for comparison between pairs of sequences. P^a Results were considered statistically significant at $P^a < 0.016$.
Friedman nonparametric test was used for statistical analysis of the three sequences. P^b Results were considered statistically significant at $P^b < 0.05$.
* Statistically significant
CAIPIRINHA = controlled aliasing in parallel imaging results in a higher acceleration; GA = golden angle; GRE = gradient-recalled echo; ILAB = interleaved angle-bisection; VIBE = volumetric interpolated breath-hold examination

Table 5. Results of Quantitative Analysis of Three, Motion-Resistant Sequences in Cooperative Patients

Parameters	3D GRE VIBE with CAIPIRINHA	3D radial GRE		P^a			P^b
		GA	ILAB	3D GRE VIBE with CAIPIRINHA vs. 3D radial GRE with GA	3D GRE VIBE with CAIPIRINHA vs. 3D radial GRE with ILAB	3D radial GRE with GA vs. 3D radial GRE ILAB	
SI of liver	366.15 ± 116.76	456.42 ± 138.08	465.35 ± 146.14	< 0.001*	< 0.001*	0.007*	< 0.001*
SI of lesion	200.80 ± 78.27	236.38 ± 85.25	236.53 ± 84.54	< 0.001*	< 0.001*	1	< 0.001*
SD of background	3.52 ± 1.43	4.32 ± 1.61	3.93 ± 1.66	0.015*	0.419	0.123	0.007*
SNR of liver	116.73 ± 53.31	116.40 ± 49.42	133.17 ± 58.16	1	0.122	0.004*	0.019*
CNR							
Total	47.79 ± 29.18	53.90 ± 30.81	62.60 ± 33.55	0.237	0.15	0.15	0.02*
Malignant	40.89 ± 21.71	42.39 ± 21.73	52.92 ± 29.99	NA	NA	NA	0.066
Benign	55.89 ± 35.03	67.45 ± 34.85	73.99 ± 34.77	0.163	0.055	0.287	0.025*
SI of fat	101.92 ± 36.90	90.24 ± 25.54	86.63 ± 25.40	0.028	0.002*	< 0.001*	< 0.001*
SD of fat	12.92 ± 4.77	9.05 ± 3.09	8.65 ± 3.07	< 0.001*	< 0.001*	0.494	< 0.001*
Percentage of SD	13.87 ± 5.70	10.43 ± 3.37	10.35 ± 3.19	< 0.001*	< 0.001*	1	< 0.001*

Values are the mean ± standard deviation. NA: Post hoc paired t-test with Bonferroni correction was not available.
Post hoc paired t-test with Bonferroni correction was used for comparison between pairs of sequences. P^a Results were considered statistically significant at $P^a < 0.016$.
Repeated measures analysis of variance was used for statistical analysis of the three sequences. P^b Results were considered statistically significant at $P^b < 0.05$.
* Statistically significant
CAIPIRINHA = controlled aliasing in parallel imaging results in a higher acceleration; CNR = contrast-to-noise ratio; GA = golden angle; GRE = gradient-recalled echo; ILAB = interleaved angle-bisection; SD = standard deviation; SI = signal intensity; SNR = signal-to-noise ratio; VIBE = volumetric interpolated breath-hold examination

Table 6. Results of Quantitative Analysis of Three, Motion-Resistant Sequences in Uncooperative Patients

Parameters	3D GRE VIBE with CAIPIRINHA	3D radial GRE		P^a			P^b
		GA	ILAB	3D GRE VIBE with CAIPIRINHA vs. 3D radial GRE with GA	3D GRE VIBE with CAIPIRINHA vs. 3D radial GRE with ILAB	3D radial GRE with GA vs. 3D radial GRE ILAB	
SI of liver	326.96 ± 98.48	388.70 ± 112.66	396.60 ± 117.63	< 0.001*	< 0.001*	< 0.001*	< 0.001*
SI of lesion	204.35 ± 62.74	216.02 ± 64.23	213.68 ± 65.27	NA	NA	NA	0.422
SD of background	19.84 ± 9.62	3.26 ± 1.25	3.37 ± 1.34	< 0.001*	< 0.001*	0.198	< 0.001*
SNR of liver	23.70 ± 18.46	131.56 ± 56.54	131.69 ± 58.91	< 0.001*	< 0.001*	0.982	< 0.001*
CNR							
Total	11.16 ± 10.53	58.16 ± 36.87	64.88 ± 43.73	0.001*	0.001*	0.083	0.001*
Malignant	10.94 ± 10.69	52.96 ± 31.68	59.23 ± 39.28	0.003*	0.004*	0.163	0.002*
Benign	12.35 ± 13.54	86.80 ± 65.86	95.97 ± 72.32	NA	NA	NA	0.135
SI of fat	103.45 ± 34.93	77.26 ± 23.51	73.83 ± 20.09	0.001*	0.001*	0.014*	< 0.001*
SD of fat	15.06 ± 5.87	7.44 ± 1.95	7.28 ± 1.91	0.001*	0.001*	1	< 0.001*
Percentage of SD	15.74 ± 7.04	10.11 ± 2.91	10.09 ± 2.19	0.002*	0.001*	1	0.002*

Values are the mean ± standard deviation. NA: Post hoc paired t-test with Bonferroni correction was not available.

Post hoc paired t-test with Bonferroni correction was used for comparison between pairs of sequences. P^a Results were considered statistically significant at $P^a < 0.016$.

Repeated measures analysis of variance was used for statistical analysis of the three sequences. P^b Results were considered statistically significant at $P^b < 0.05$.

* Statistically significant

CAIPIRINHA = controlled aliasing in parallel imaging results in a higher acceleration; CNR = contrast-to-noise ratio; GA = golden angle; GRE = gradient-recalled echo; ILAB = interleaved angle-bisection; SD = standard deviation; SI = signal intensity; SNR = signal-to-noise ratio; VIBE = volumetric interpolated breath-hold examination

GRE with GA and the 3D radial GRE with ILAB had excellent fat suppression with uniformity, compared to the 3D GRE with CAIPIRINHA. The fat percentage SD of SI with a 3D radial GRE sequence with GA and a 3D radial with ILAB was significantly lower than that with the 3D GRE with CAIPIRINHA, i.e. P = 0.002 and 0.001, respectively. There was no significant difference between the 3D radial GRE with GA and the 3D radial GRE ILAB.

DISCUSSION

The CAIPIRINHA technique uses a unique k-space sampling pattern to reduce the aliasing artifact, and thereby improve imaging quality beyond the effect of standard parallel image techniques. The acquired k-space samplings are offset from the normal grid-like sampling by shifting the sampling positions of alternate rows with respect to the partition-encoding direction (7, 9, 10). This technique can save the acquisition time and the breath-holding time more effectively than the generalized auto calibrating partially parallel acquisition (GRAPPA) technique (8-10, 13). In cooperative patients, our study showed that the 3D GRE with CAIPIRINHA was superior to 3D radial GRE with GA and ILAB for all qualitative analyses. The merits of 3D GRE with CAIPIRINHA are a shorter image acquisition time (approximately 10-14 seconds) and better image quality in patients with well-controlled breathing. However, in uncooperative patients, two, 3D radial GRE sequences showed a higher grade than 3D GRE with CAIPIRINHA, especially in regard to some significant items, such as the clarity of intrahepatic vessels and lesion conspicuity, which recorded less than three points and which indicates uninterpretable, poor image quality in 3D GRE with CAIPIRINHA. Therefore, our results showed that 3D GRE with CAIPIRINHA can be used in a limited manner in uncooperative patients. In the future, further evolution of 3D GRE with CAIPIRINHA using compressed sensing, or time-resolved imaging with stochastic trajectories, may enable motionless MR images possible in some uncooperative patients, who cannot comply with the 10-second, breath-holding requirement (16).

The 3D radial GRE sequence (3D Radial GRE) is a motion-resistant protocol that uses the radial k-space sampling system. With the radial acquisition methods, the radial spokes overlap in the k-space center, which averages the

information and reduces the motion artifact (1, 7, 11, 16). Therefore, the use of this technique could provide higher quality images, which could be especially useful in patients which have breath-holding difficulties or in those with poor compliance, despite requiring a substantial amount of acquisition time (17, 18). Our results also showed that the 3D radial GRE with GA, and the 3D radial GRE with ILAB had better image quality than the 3D GRE with CAIPIRINHA and that there we statistically significant differences between the two; 3D radial GRE sequences and 3D GRE with CAIPIRINHA ($P < 0.016$) for all qualitative analysis except streak artifact in uncooperative patients.

A previous study showed that 3D radial GRE with GA, in combination with compressed sensing in multiphase liver MR imaging, leads to more uniform coverage of the k-space for a small number of spokes (approximately 100 radial spokes) than ILAB acquisition with a short angular distance (1, 11-15). As a result, 3D radial GRE with GA, using randomly flickering patterns for under sampling acquisition, had higher image quality and enhancement quality than those of 3D GRE with ILAB (13). On the other hand, our study demonstrated that two, different radial acquisition methods, on most qualitative and quantitative parameters, did not differ significantly in either the cooperative or uncooperative patients. These results may be attributed to the use of a large number of radial spokes (1024 radial spokes) under the free-breathing circumstance, and thus result in being able to fill the k-space more fully and uniformly (13) and to achieve a similar performance in both 3D radial GRE with GA and ILAB.

Our study showed that the SNR of liver and lesion-to-liver CNR of the free-breathing, 3D radial GRE sequence in uncooperative patients, were significantly higher than those of 3D GRE with CAIPIRINHA. In 3D GRE with CAIPIRINHA, the background noise was higher than that of 3D radial GRE owing to patient movement, which leads to a decreased SNR of liver and CNR of lesions. Parallel imaging, such as 3D GRE with CAIPIRINHA, can significantly decrease the SNR due to a reduction in the number of collected data. For parallel imaging, SNR is proportional to $1/\sqrt{R}$ (R is the acceleration factor) (19). The application of 3D GRE with CAIPIRINHA using an acceleration factor of 4 results in a two-fold reduction in the SNR (7, 9, 16). In our study, the CNR of malignant tumors differ, particularly, between the free-breathing, 3D radial GRE sequence and 3D GRE with CAIPIRINHA in uncooperative patients. Therefore, it could be important to use the free-breathing, 3D radial GRE sequence in uncooperative patients in order to be able to diagnose these malignant tumors. In addition, in our study the SI and SD of fat in two, 3D radial GRE sequences were significantly lower compared with those in 3D GRE CAIPIRINHA. The suppression of fat seems to be more homogenous in the 3D radial GRE sequence, as the SD of fat showed a lower value. Fat suppression can increase the CNR because normal liver usually contains fat (20).

We recognize that our study had several limitations. First, image acquisition timing differs with the three sequences. It was difficult to precisely match the image acquisition time, because of the free-breathing manner of 3D, radial GRE sequences. We attempted to minimize the difference of SI caused by the time effect by allowing continuous MR scanning (first scan: 3D GRE with CAIPIRINHA; second scan: 3D radial GRE with GA; third scan: 3D radial GRE with ILAB). Second, accurate measurements of the SNR and lesion-to-liver CNR, according to a well-established method, may have suffered from inhomogeneous distribution of noise due to parallel imaging and streak artifacts. We attempted to minimize any inherent bias by measuring noise in the "empty space" of the image dataset. Third, the cooperativeness of patients and the determination of scan protocols were subjectively decided by only scanning technologists. However, we tried to perform the test after sufficient confirmation that the patients could follow the instruction and hold their breath during precontrast, and in-phase/out-of-phase sequence. Fourth, we compared three sequences only on the hepatobiliary phase. Further studies will be needed on the dynamic phase.

In conclusion, in uncooperative patients, the use of 3D, radial GRE sequences can improve the image quality, compared with that of the 3D GRE with CAIPIRINHA, despite whatever data acquisition methods, i.e. ILAB or GA acquisitions, are used. And the 3D GRE imaging with CAIPIRINHA is applicable to patients without breath-holding difficulties.

Acknowledgments

We thank Bonnie Hami, MA (USA) for her editorial assistance in preparing the manuscript. We thank Siemens Healthcare for their research support in the form of hardware and software.

REFERENCES

1. Bamrungchart S, Tantaway EM, Midia EC, et al. Free breathing three-dimensional gradient echo-sequence with radial data sampling (radial 3D-GRE) examination of the

pancreas: Comparison with standard 3D-GRE volumetric interpolated breathhold examination (VIBE). J Magn Reson Imaging 2013;38:1572-1577
2. Birchard KR, Semelka RC, Hyslop WB, et al. Suspected pancreatic cancer: evaluation by dynamic gadolinium-enhanced 3D gradient-echo MRI. AJR Am J Roentgenol 2005;185:700-703
3. Kim BS, Angthong W, Jeon YH, Semelka RC. Body MR imaging: fast, efficient, and comprehensive. Radiol Clin North Am 2014;52:623-636
4. Rofsky NM, Lee VS, Laub G, et al. Abdominal MR imaging with a volumetric interpolated breath-hold examination. Radiology 1999;212:876-884
5. Semelka RC, Helmberger TK. Contrast agents for MR imaging of the liver. Radiology 2001;218:27-38
6. Semelka RC, Martin DR, Balci NC. Magnetic resonance imaging of the liver: how I do it. J Gastroenterol Hepatol 2006;21:632-637
7. Kim BS, Lee KR, Goh MJ. New imaging strategies using a motion-resistant liver sequence in uncooperative patients. Biomed Res Int 2014;2014:142658
8. Park YS, Lee CH, Kim IS, et al. Usefulness of controlled aliasing in parallel imaging results in higher acceleration in gadoxetic acid-enhanced liver magnetic resonance imaging to clarify the hepatic arterial phase. Invest Radiol 2014;49:183-188
9. Wright KL, Harrell MW, Jesberger JA, et al. Clinical evaluation of CAIPIRINHA: comparison against a GRAPPA standard. J Magn Reson Imaging 2014;39:189-194
10. Yu MH, Lee JM, Yoon JH, Kiefer B, Han JK, Choi BI. Clinical application of controlled aliasing in parallel imaging results in a higher acceleration (CAIPIRINHA)-volumetric interpolated breathhold (VIBE) sequence for gadoxetic acid-enhanced liver MR imaging. J Magn Reson Imaging 2013;38:1020-1026
11. Azevedo RM, de Campos RO, Ramalho M, Heredia V, Dale BM, Semelka RC. Free-breathing 3D T1-weighted gradient-echo sequence with radial data sampling in abdominal MRI: preliminary observations. AJR Am J Roentgenol 2011;197:650-657
12. Chandarana H, Block TK, Rosenkrantz AB, et al. Free-breathing radial 3D fat-suppressed T1-weighted gradient echo sequence: a viable alternative for contrast-enhanced liver imaging in patients unable to suspend respiration. Invest Radiol 2011;46:648-653
13. Chandarana H, Feng L, Block TK, et al. Free-breathing contrast-enhanced multiphase MRI of the liver using a combination of compressed sensing, parallel imaging, and golden-angle radial sampling. Invest Radiol 2013;48:10-16
14. Kim KW, Lee JM, Jeon YS, et al. Free-breathing dynamic contrast-enhanced MRI of the abdomen and chest using a radial gradient echo sequence with K-space weighted image contrast (KWIC). Eur Radiol 2013;23:1352-1360
15. Song HK, Dougherty L. Dynamic MRI with projection reconstruction and KWIC processing for simultaneous high spatial and temporal resolution. Magn Reson Med 2004;52:815-824
16. Runge VM, Richter JK, Heverhagen JT. Speed in clinical magnetic resonance. Invest Radiol 2017;52:1-17
17. Chandarana H, Block KT, Winfeld MJ, et al. Free-breathing contrast-enhanced T1-weighted gradient-echo imaging with radial k-space sampling for paediatric abdominopelvic MRI. Eur Radiol 2014;24:320-326
18. Shin HJ, Kim MJ, Lee MJ, Kim HG. Comparison of image quality between conventional VIBE and radial VIBE in free-breathing paediatric abdominal MRI. Clin Radiol 2016;71:1044-1049
19. Pruessmann KP, Weiger M, Scheidegger MB, Boesiger P. SENSE: sensitivity encoding for fast MRI. Magn Reson Med 1999;42:952-962
20. Mitchell DG, Vinitski S, Saponaro S, Tasciyan T, Burk DL Jr, Rifkin MD. Liver and pancreas: improved spin-echo T1 contrast by shorter echo time and fat suppression at 1.5 T. Radiology 1991;178:67-71